



Validation of a Robotic Testing Procedure for Shoulder *In-Vitro* Biomechanical Testing

Florent Moissenet^{1,3*}, Clément Rastoll², David Gonzalez², Noria Foukia², Michel Lauria², Stéphane Armand³, Jean-Yves Beaulieu³ and Nicolas Holzer³

¹Biomechanics Laboratory, Geneva University Hospitals and University of Geneva, Switzerland

²Geneva School of Engineering, Architecture and Landscape - HEPIA, Switzerland

³Kinesiology Laboratory, Geneva University Hospitals and University of Geneva, Switzerland

⁴Department of Surgery, Geneva University Hospitals, Switzerland

Abstract

Cadaveric joint simulators are commonly used to explore native and pathological joint function as well as to test medical devices. Recently, robotic manipulators have been proposed as a new gold standard for *in vitro* biomechanical testing as they offer higher possibilities than Universal Testing Machines (UTM) in terms of Degrees of Freedom (DOF). However, current protocols remain conducted in extra-corporal conditions by fixing one segment of a diarthrodial joint while mobilizing the other segment. Moreover, induced motions are commonly not specimen-specific and do not respect related joint kinematic constraints and physiologic boundaries. In this study, using an industrial robotic manipulator, an intra-corporal condition procedure was defined. This procedure allows 1) the analysis of the shoulder girdle full kinematic chain, 2) the replication of specimen-specific humerus motions initially induced by an operator. On the 10 shoulders tested, the robotic manipulator was able to perform requested end-effector motions with a reliability of 0.28 ± 0.57 mm and $0.15 \pm 0.25^\circ$, and fidelity of 0.27 ± 0.56 mm and $0.22 \pm 0.28^\circ$. This procedure will be used in the future to explore joint function as well as to test medical devices, on the shoulder girdle and potentially other joints.

Keywords: Robotic testing; Biomechanical testing; Cadaveric joint; Universal testing machines

OPEN ACCESS

*Correspondence:

Florent Moissenet, Biomechanics Laboratory, Geneva University Hospitals and University of Geneva, Geneva, Switzerland,
E-mail: florent.moissenet@unige.ch

Received Date: 31 May 2022

Accepted Date: 01 Jul 2022

Published Date: 05 Jul 2022

Citation:

Moissenet F, Rastoll C, Gonzalez D, Foukia N, Lauria M, Armand S, et al. Validation of a Robotic Testing Procedure for Shoulder *In-Vitro* Biomechanical Testing. *World J Surg Surgical Res.* 2022; 5: 1392.

Copyright © 2022 Florent Moissenet.

This is an open access article distributed under the Creative Commons Attribution License, which permits unrestricted use, distribution, and reproduction in any medium, provided the original work is properly cited.

Introduction

Cadaveric joint simulators are commonly used to explore the native and pathological joint function [1] as well as to test medical devices [2]. While Universal Testing Machines (UTM) have been recognized these last decades as a standard for joint biomechanical testing [3], the use of robotic manipulators is proposed as a new gold standard for *in vitro* biomechanical testing [4]. This is mainly motivated by the fact that they offer higher possibilities than UTM in terms of Degrees of Freedom (DOF). This is essential for the assessment of complex joints such as the shoulder [5]. Several clinical applications have thus been proposed to assess acromioclavicular joint stability [6], to evaluate the influence of a reverse shoulder prosthesis design on scapula notching [7], or to characterize percutaneous osseointegrated implant systems [5].

However, most of the current protocols are conducted in extra-corporal conditions by rigidly fixing one segment (e.g. the scapula) of a diarthrodial joint (e.g. the acromioclavicular joint) while inducing a motion on the other segment (e.g. the clavicle) [6,7]. Hence, only few studies have explored the use of robotic manipulators on kinematic chains [8,9] and, to the best of our knowledge, such an approach has never been applied on the shoulder girdle. Indeed, exploring this whole kinematic chain is challenging as it is composed of three bones (i.e. humerus, scapula, clavicle) and four joints (i.e. glenohumeral, sternoclavicular, acromioclavicular and scapulohoracic), but also regarding the large available range of motion [10].

Using a robotic manipulator, induced motions are commonly defined around anatomical axes [6,11]. These axes are sometimes defined through well recognized recommendations (e.g. International Society of Biomechanics (ISB) recommendations for segment coordinate axes definition) to allow for interspecimen and intersession comparisons [12,13]. In some other studies, datasets obtained from healthy participants are used to replicate motion patterns observed during various dynamic tasks [5,8]. Such an approach is interesting to reproduce complex *in vivo* human

motions, but may be subject to measurement errors due to soft tissue artifacts acting on motion capture sensors (e.g. reflective cutaneous markers) [14]. Furthermore, unlike manually-induced motions that may respect specimen-specific kinematic constraints (e.g. bony or soft tissue constraints that may limit further joint motion) [1], *in vivo* human motions applied by the operator on the specimen have to be adapted to the specimen joint characteristics. This can be done by a scaling data procedure [15] or by the use of a 6-axis universal force-moment sensor to limit forces and moments applied by the manipulator on the joint [7]. However, to the best of our knowledge, manually-induced motions recorded on the investigated specimen have never been directly replicated by the use of a robotic manipulator. Whereas such an application can allow for replication of specific motions (e.g. intraoperative joint assessment performed by the surgeon) in a higher repeatable manner than during manually-induced motions [16,17].

The first objective of this study was to develop an advanced joint testing procedure using an industrial robotic manipulator to explore the shoulder girdle kinematics during specimen-specific humerus motions in native intra-corporal conditions. The second objective was to assess the procedure reliability, validity and fidelity to replicate a set of consecutive quasi-static humerus motions. These motions were initially manually-induced on the specimen by an experienced operator. Errors below 1 mm and 1° were expected regarding the reliability and fidelity of the manipulator end-effector position and orientation, respectively.

Materials and Methods

Robotic manipulator

A KUKA LBR IIWA 14 R820 (KUKA Robotics Corp, Germany) redundant robotic manipulator was used in this study (Figure 1). This 7 DOF manipulator has a manufacturer reported maximal payload of 14 kg and an end-effector position reliability of 0.1 mm.

Specimen preparation

Five fresh-frozen, un-embalmed adult whole cadavers (77.4 ± 9.99 years, Table 1) were obtained for the study. None of the shoulders

had a degenerative joint disease or previous ligamentous injury confirmed by direct inspection and radiographs before experiments. All specimens were acquired at the Anatomy Teaching Unit of the Geneva Faculty of Medicine. These specimens were all selected from the body donation program of the University of Geneva. The Cantonal Commission for Research Ethics approved this study (2020-00598). All procedures were performed in accordance with the ethical standards of the institutional research committee and with the 1964 Helsinki Declaration and later amendments.

Specimens were stored at -20° and thawed at room temperature during approximately 72 h prior to testing. They were positioned in a sitting position on a custom-made vertical support with wedges at cervical and lumbar levels to avoid any conflict between scapula and support (Figure 1). Straps were tied at cervical and lumbar levels to stabilize specimens.

Manipulator workspace and humerus reachable workspace fitting

The Thoracic Coordinate System (TCS, Figure 2) was used to describe the specimen position and orientation. It was defined following ISB recommendations 12 using the reflective cutaneous marker 3D trajectories defined thereafter. Specimen position and orientation, with respect to the manipulator coordinate system (MCS, Figure 2), were crucial parameters to ensure that the Humerus Reachable Workspace (HRW) was contained in the Robotic Manipulator Workspace (RMW) for humerus motion replication.

RMW was defined as the volume between an inferior sphere and a superior sphere centered at the manipulator workspace centre, with a radius equal to the distance between joint axes 2 and 4, and to the distance between joint axes 2 and 6, respectively (Figure 3). The between axes distances were based on the manufacturer documentation [18]. Security margins, set at 20 mm, were added to the spheres radius.

The maximal HRW was defined by estimating the Glenohumeral Joint Centre (GJC) and the Elbow Joint Centre (EJC) 3D trajectories during manual humerus mobilization in the full range of motion

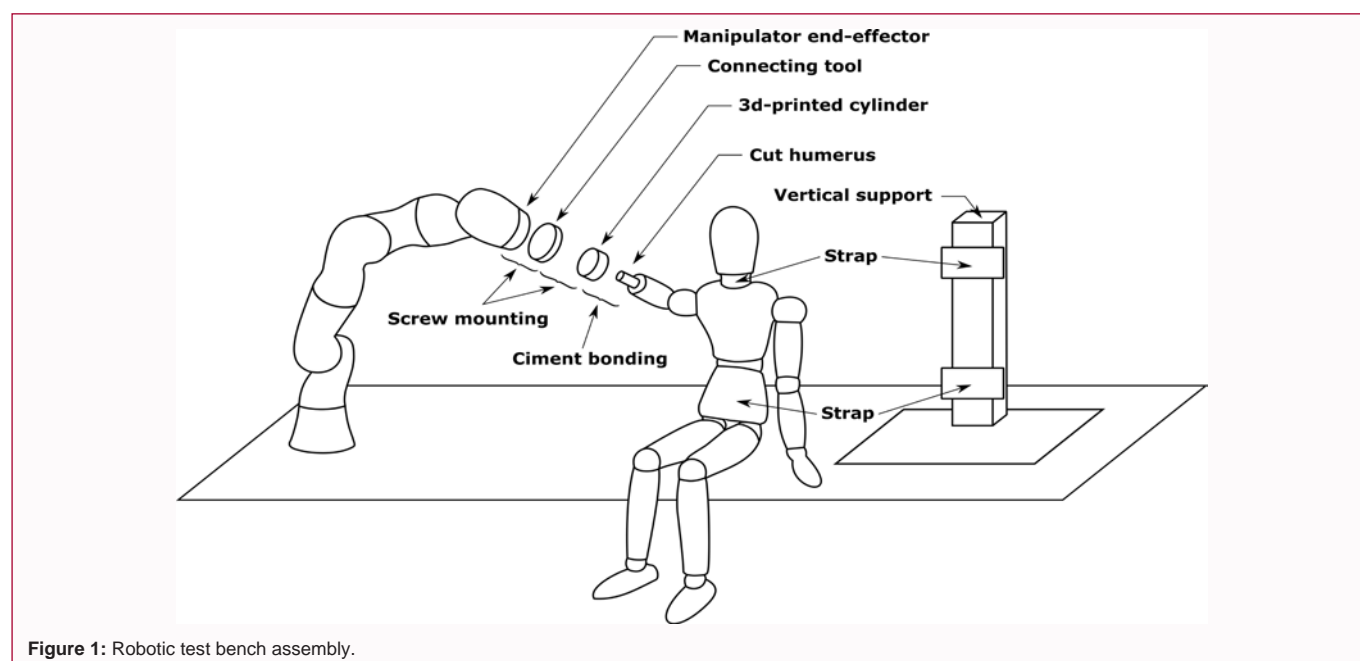


Figure 1: Robotic test bench assembly.

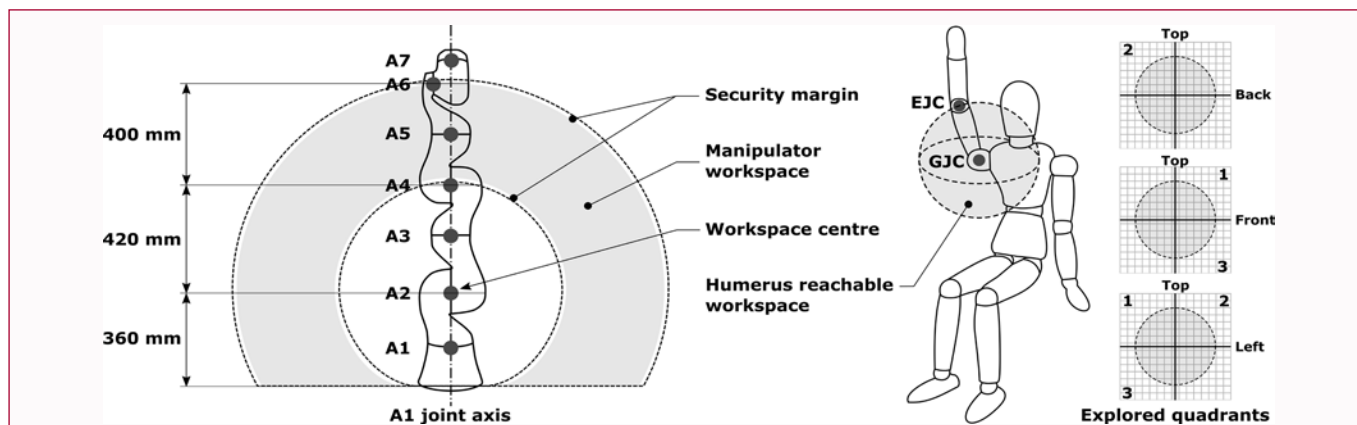


Figure 2: Segment coordinate systems used in the analysis (MCS: Manipulator Coordinate System; TCS: Thorax Coordinate System, ECS: End-Effector Coordinate System). ECS is shared between the manipulator end-effector and the 3d-printed humeral cylinder.

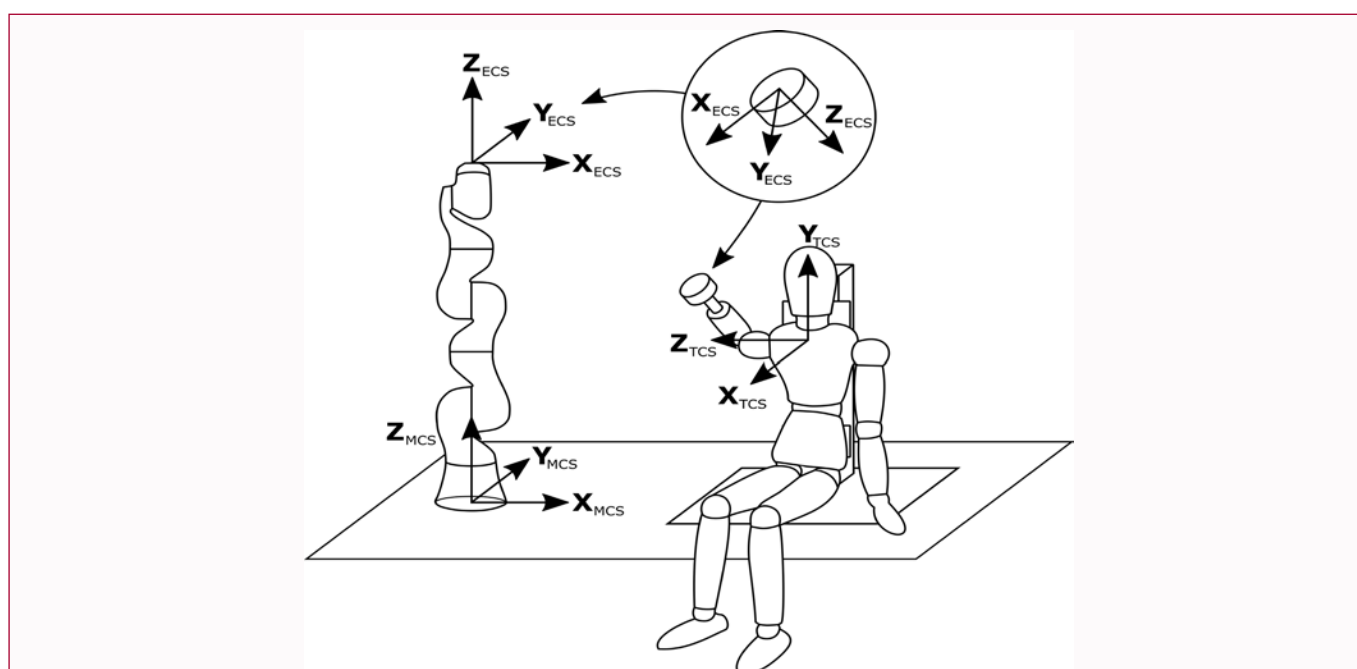


Figure 3: Illustration of the manipulator workspace (on the left) and humerus reachable workspace (on the right). The manipulator workspace is a volume defined by a 340° revolution of the grey surface around the A1 joint axis (Ai: Joint Centre of the Axis i). The humerus reachable workspace is defined by 3 quadrants (1, 2 and 3) of the grey sphere (GJC: Glenohumeral Joint Centre; EJC: Elbow Joint Centre).

in the following quadrants: Antero-lateral superior (quadrant 1), Antero-medial superior (quadrant 2) and Antero-lateral inferior (quadrant 3) (Figure 3). Motions consisted in shoulder flexion-extension, abduction-adduction, internal-external rotation (at 0° of flexion), horizontal flexion-extension, vertical traction and horizontal compression. Care was taken not to influence the internal-external humerus rotation during extension and abduction. Following ISB recommendations [12], GJC was defined by regression equations [19] and EJC as the midpoint between medial and lateral humeral epicondyles. For that, a set of reflective cutaneous markers were placed on 7 bony landmarks (SJN: Jugular Notch; SXS: Xiphisternal Joint; CAJ: Acromioclavicular Joint; CV7: Cervical Vertebrae 7; TV8: Thoracic Vertebrae 8, HLE: Lateral Humeral Epicondyle; HME: Medial Humeral Epicondyle) by anatomical palpation [20]. During manually-induced humerus motions, the 3D marker trajectories were recorded using a 11-camera optoelectronic system sampled at 100 Hz (Oqus 5, Qualisys, Sweden), gap-filled and filtered (2nd order

Butterworth filter, 6 Hz cut-off).

Due to a limited RMW, it was necessary to reduce the humerus length to fit the HRW into the manipulator workspace. For that, a submaximal HRW was computed for each virtual point (HCi) equally distributed every 1 cm along the humerus longitudinal axis between GJC and EJC. These virtual points aimed at representing potential humerus transection locations. Each resulting HRW was defined as the 3 previously defined quadrants of the minimal sphere centered at GJC including all trajectories of the related HCi point. GJC, EJC and HC_i points were all expressed in MCS (Figure 2). For each HRW, a custom-made iterative algorithm (Matlab R2018b, The Math Works, USA) was used to compute all TCS positions and orientations allowing the HRW to be contained in the RMW. The resulting solution space was composed of various humerus cut lengths and TCS positions and orientations. For each shoulder, the applied solution (Table 1) was selected so as to keep the longest humerus length while using a

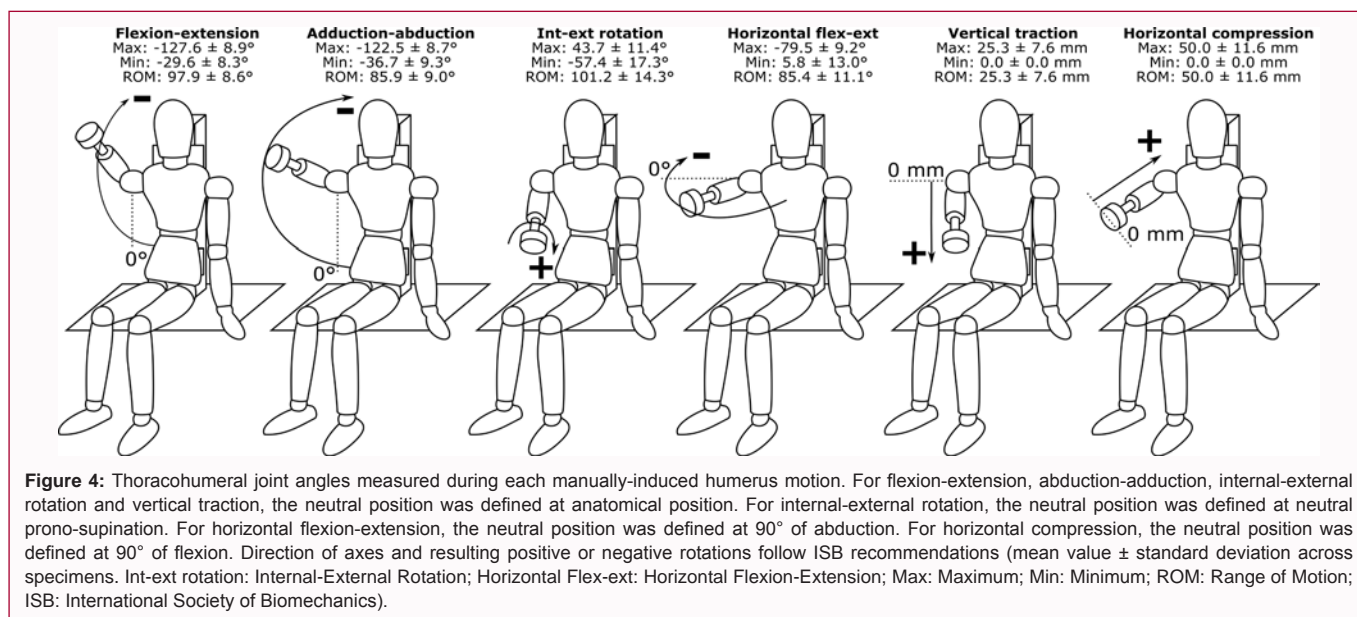


Figure 4: Thoraco humeral joint angles measured during each manually-induced humerus motion. For flexion-extension, abduction-adduction, internal-external rotation and vertical traction, the neutral position was defined at anatomical position. For internal-external rotation, the neutral position was defined at neutral prono-supination. For horizontal flexion-extension, the neutral position was defined at 90° of abduction. For horizontal compression, the neutral position was defined at 90° of flexion. Direction of axes and resulting positive or negative rotations follow ISB recommendations (mean value ± standard deviation across specimens. Int-ext rotation: Internal-External Rotation; Horizontal Flex-ext: Horizontal Flexion-Extension; Max: Maximum; Min: Minimum; ROM: Range of Motion; ISB: International Society of Biomechanics).

Table 1: Details about the specimens and applied solutions in terms of position (in the MCS) and orientation (around the Z_{MCS} , 0° corresponds to X_{MCS} and Z_{TCS} aligned) of the specimen and humerus cut length, for each shoulder of each specimen (MCS: Manipulator Coordinate System; TCS: Thorax Coordinate System).

Specimen (ID)	Gender (F/M)	Age (years)	Height (cm)	Weight (kg)	Shoulder (side)	Position and orientation				Cut Length (cm)
						TX (cm)	TY (cm)	TZ (cm)	R (°)	
RS001	Female	94	158	56.4	Right	80	-10	62	140	17.6
					Left	81	10	62.5	40	19.6
RS002	Female	74	155	55	Right	76	-50	65.5	120	13.5
					Left	73	13	65	45	12.2
RS003	Female	76	165	66	Right	80	-16	57	135	15.9
					Left	80	10	51	30	17.6
RS004	Female	76	158	73	Right	80	-16	52	130	13.3
					Left	79	1	57	50	15.3
RS005	Female	67	165	60	Right	80	-14	52	130	14.2
					Left	80	7	55	45	15.5

median TCS position and orientation across all solutions related to the selected humerus cut length.

Each humerus was then transected, potted in a custom 3D-printed cylinder (ABS thermoplastic polymer) by use of bone cement (Palacos LV, Heraeus, Germany), and rigidly mounted via a custom fixture to the manipulator end-effector (Figure 1). All soft tissues (e.g. muscles, ligaments, joint capsules) were left intact along the whole shoulder girdle. The specimen position and orientation was adjusted and rigidly secured to the table using clamps.

Manipulator motion planning

During surgery, shoulder Range of Motion (ROM) is commonly assessed using manual testing by passively mobilizing the humerus until bony or soft tissue constraints prevent further motion. In order to reproduce this intraoperative assessment, manually-induced humerus motions were replicated by the manipulator. For that, a new set of reflective markers was used to record manually-induced motions of the transected humerus. To obtain true kinematics, free from soft tissue artifacts, these markers were put on the 3D-printed cylinder (rigidly secured to the bone) to define its related coordinate system. The cylinder design ensured that the axes of its coordinate system

were coaxial with those of the manipulator end-Effector Coordinate System (ECS, Figure 2). The rigid transformation between these coordinate systems was thus defined based on geometry features.

Once again, the operator manipulated the humerus using the same motions as previously defined. Three-dimensional marker trajectories were gap-gilled and filtered (2nd order Butterworth filter, 6 Hz cut-off) and used to compute the matrix corresponding to the trajectory of the end-effector centre and the quaternion of its 3D orientation, both discretized into 100 waypoints for each manually-induced motion. These data were then sent to ROS (Robot Operating System, version 16.04.6 “Kinetic”) and the manipulator motion planning (i.e. the angular value of each robot joint axis at each timeframe) was computed by inverse kinematics using the Open Rave IK Fast solver (version 0.9.0). For each humerus motion, the resulting trajectory planning was sent to the manipulator through the IIWA stack library [21,22].

Replication of manually-induced humerus motions

Manually-induced humerus motions were finally replicated by the manipulator (6 cycles per motion) in a quasi-static condition (maximal rate of 5°.s⁻¹) using the embedded KUKA Sunrise. OS

Table 2: Reliability and validity of the manipulator joint axis angles (metrics are reported by their mean value \pm standard deviation across cycles and specimens. FE: Flexion-Extension; AA: Abduction-Adduction; IER: Internal-External Rotation; HFE: Horizontal Flexion-Extension; VT: Vertical Traction; HC: Horizontal Compression).

		Manipulator joint axes							Legend
		Joint A1	Joint A2	Joint A3	Joint A4	Joint A5	Joint A6	Joint A7	
		Angle (°)	Angle (°)	Angle (°)	Angle (°)	Angle (°)	Angle (°)	Angle (°)	
FE	Reliability	0.20 \pm 0.21	0.26 \pm 0.35	0.25 \pm 0.25	0.36 \pm 0.36	0.61 \pm 0.96	0.44 \pm 0.77	0.52 \pm 0.67	
	Validity	0.43 \pm 0.33	0.46 \pm 0.43	0.44 \pm 0.32	0.90 \pm 0.57	0.90 \pm 1.19	0.79 \pm 0.97	0.87 \pm 0.82	
AA	Reliability	0.20 \pm 0.13	0.24 \pm 0.19	0.26 \pm 0.19	0.28 \pm 0.20	0.52 \pm 0.39	0.41 \pm 0.34	0.48 \pm 0.39	
	Validity	0.37 \pm 0.23	0.39 \pm 0.21	0.40 \pm 0.22	0.68 \pm 0.33	0.83 \pm 0.46	0.71 \pm 0.45	0.82 \pm 0.41	<0.25°
IER	Reliability	0.09 \pm 0.08	0.08 \pm 0.05	0.12 \pm 0.11	0.09 \pm 0.06	0.17 \pm 0.10	0.15 \pm 0.10	0.43 \pm 0.37	
	Validity	0.09 \pm 0.09	0.08 \pm 0.06	0.12 \pm 0.12	0.08 \pm 0.06	0.15 \pm 0.11	0.12 \pm 0.10	0.51 \pm 0.43	\geq 0.25°
HFE	Reliability	0.30 \pm 0.35	0.21 \pm 0.19	0.20 \pm 0.24	0.27 \pm 0.24	0.50 \pm 0.74	0.47 \pm 0.50	0.39 \pm 0.53	
	Validity	0.49 \pm 0.43	0.33 \pm 0.22	0.36 \pm 0.42	0.53 \pm 0.27	0.87 \pm 1.12	0.71 \pm 0.56	0.80 \pm 0.92	\geq 0.50°
VT	Reliability	0.04 \pm 0.03	0.06 \pm 0.11	0.05 \pm 0.05	0.08 \pm 0.09	0.09 \pm 0.09	0.09 \pm 0.17	0.10 \pm 0.13	
	Validity	0.05 \pm 0.05	0.08 \pm 0.18	0.07 \pm 0.08	0.09 \pm 0.13	0.12 \pm 0.14	0.11 \pm 0.27	0.14 \pm 0.19	\geq 0.75°
HC	Reliability	0.09 \pm 0.10	0.08 \pm 0.09	0.06 \pm 0.07	0.07 \pm 0.06	0.17 \pm 0.20	0.23 \pm 0.28	0.13 \pm 0.11	
	Validity	0.12 \pm 0.15	0.10 \pm 0.12	0.06 \pm 0.09	0.07 \pm 0.10	0.20 \pm 0.30	0.25 \pm 0.34	0.14 \pm 0.18	\geq 1.00°

(version 1.10.0.8, KUKA, Switzerland). Joint axis angles and end-effector Cartesian poses were stored for each cycle at 100 Hz.

Statistical analysis

In order to assess the manipulator ability to replicate manually-induced humerus motions, the following analyses were conducted.

The reliability and validity of the manipulator joint angles were assessed by comparing, for each humerus motion, these angles with their average value across all cycles, and with the planned trajectory, respectively. The reliability and fidelity of the end-effector position and orientation (and thus the humerus position and orientation) were assessed by comparing, for each humerus motion, these parameters with their average value across all cycles, and with the position and orientation measured during manually-induced physiological humerus motion, respectively.

As the motion velocity was not constrained, it may have varied between cycles and between manipulator-induced and manually-induced motions. Thus, a Dynamic Time Warping (DTW) approach was used to map the compared time-series [23]. The Root Mean Square Difference (RMSD) was then computed between the resulting mapped data for each humerus motion cycle. The RMSD related to reliability, validity and fidelity were finally reported, for each humerus motion, by their mean and standard deviation values across cycles and specimens.

Results

Manually-induced humerus motions

The average thoracohumeral joint (i.e. humerus relative to the thorax) angles measured during each manually-induced humerus motion are reported in Figure 4.

Reliability and validity of the manipulator joint angles

The average RMSD related to reliability and validity were respectively $0.35 \pm 0.45^\circ$ and $0.32 \pm 0.43^\circ$ across all specimens, joints, motions and cycles (Table 2). No joint angle reached an average RMSD higher than 1° concerning reliability and validity.

Reliability and fidelity of the manipulator end-effector position

The average RMSD related to reliability and fidelity were respectively 0.28 ± 0.57 mm and 0.27 ± 0.56 mm across all specimens, joints, motions and cycles (Table 3). Only one joint angle reached an average RMSD higher than 1 mm concerning its reliability (position along the Z_{MCS} axis during flexion-extension). Concerning fidelity to the manually-induced motions, an average RMSD higher than 1 mm was observed along the X_{MCS} axis (during horizontal flexion-extension) and Z_{MCS} axis (during flexion-extension and adduction-abduction), and higher than 2 mm along the Y_{MCS} axis (during horizontal flexion-extension).

Reliability and fidelity of the manipulator end-effector orientation

The average RMSD related to reliability and fidelity were respectively $0.15 \pm 0.25^\circ$ and $0.22 \pm 0.28^\circ$ across all specimens, joints, motions and cycles (Table 3). No joint angle reached a RMSD higher than 1° concerning its reliability and fidelity.

Discussion

The key outcome of this study was the validation of testing procedure based an industrial robotic manipulator for the *in vitro* replication of manually-induced humerus motions on a native whole shoulder girdle. The present results demonstrated that the opportunities offered by robotic manipulators can be extended to complex kinematic chains in intra-corporal conditions while ensuring a high level of reliability, validity and fidelity. This feature opens new avenues in native and pathological joint function exploration as well as in medical device testing.

On average, the robotic manipulator was able to perform requested end-effector motions with a reliability of 0.28 ± 0.57 mm and $0.15 \pm 0.25^\circ$, and fidelity of 0.27 ± 0.56 mm and $0.22 \pm 0.28^\circ$. These results are generally within the targeted reliability and fidelity thresholds (i.e. <1 mm and $<1^\circ$) and may thus ensure sufficient accuracy in future studies. These results are also generally similar to those obtained from studies performed on single diarthrodial joints in extra-corporal conditions. Concerning hip and knee joints, Smith

Table 3: Reliability and fidelity of the manipulator end-effector position and orientation expressed in the manipulator coordinate system (metrics are reported by their mean value and standard deviation across cycles and specimens. FE: Flexion-Extension; AA: Abduction-Adduction; IER: Internal-External Rotation; HFE: Horizontal Flexion-Extension; VT: Vertical Traction; HC: Horizontal Compression; RXY: Orientation of X or Y axis, RZ: Orientation of Z axis).

Manipulator end-effector							Legend
		Position			Orientation		
		X (mm)	Y (mm)	Z (mm)	RXY (°)	RZ (°)	
FE	Reliability	0.10 ± 0.82	0.64 ± 0.61	1.01 ± 1.37	0.26 ± 0.44	0.35 ± 0.47	
	Fidelity	0.06 ± 0.94	0.89 ± 0.72	1.41 ± 1.41	0.36 ± 0.48	0.49 ± 0.49	
AA	Reliability	0.01 ± 0.01	0.23 ± 0.14	0.99 ± 0.59	0.27 ± 0.18	0.33 ± 0.22	
	Fidelity	0.01 ± 0.01	0.30 ± 0.14	1.28 ± 0.53	0.35 ± 0.18	0.44 ± 0.22	<0.25° or <0.25 mm
IER	Reliability	0.02 ± 0.02	0.14 ± 0.09	0.09 ± 0.06	0.22 ± 0.16	0.07 ± 0.04	
	Fidelity	0.02 ± 0.03	0.17 ± 0.11	0.11 ± 0.06	0.26 ± 0.14	0.08 ± 0.05	≥ 0.25° or ≥ 0.25 mm
HFE	Reliability	0.02 ± 0.04	0.81 ± 0.67	0.16 ± 0.14	0.10 ± 0.13	0.05 ± 0.04	
	Fidelity	1.11 ± 1.65	2.41 ± 2.25	0.73 ± 1.23	0.24 ± 0.21	0.12 ± 0.11	≥ 0.50° or ≥ 0.50 mm
VT	Reliability	0.05 ± 0.09	0.11 ± 0.14	0.23 ± 0.38	0.06 ± 0.09	0.56 ± 0.08	
	Fidelity	0.05 ± 0.08	0.14 ± 0.18	0.37 ± 0.52	0.08 ± 0.11	0.09 ± 0.12	≥ 0.75° or ≥ 0.75 mm
HC	Reliability	0.02 ± 0.02	0.28 ± 0.21	0.16 ± 0.14	0.05 ± 0.04	0.04 ± 0.06	
	Fidelity	0.05 ± 0.25	0.31 ± 0.25	0.29 ± 0.76	0.05 ± 0.05	0.06 ± 0.11	≥ 1.00° or ≥ 1.00 mm

et al. [24] reported a reliability of 0.2 mm and 0.2° while Darcy et al. [25] reported a reliability of 0.3 mm and 0.1°, respectively. Concerning shoulder joint, mean absolute errors reported in our study in terms of position and orientation were always below 5% of the explored joint range of motion. These values are in line with those of Aliaj et al. [5] study. The values reported by Lee et al. [6] are lower, with a reliability of 0.03 mm and an accuracy of 0.11 mm and 0.13°. However, the experimentations were performed in a smaller range of motion than in the present study (i.e. translations ranging between 1.3 mm and 17.4 mm). In our results, it appeared that horizontal flexion-extension was more subject to errors than other humerus motions. Practically, this motion was often close to the manipulator workspace boundaries. Resulting errors could thus be reduced by decreasing the requested range of motion. In particular the maximal humerus horizontal flexion which tended to put the manipulator arm in full extension.

According to the manufacturer specifications, the KUKA LBR IIWA 14 R820 has an instrumental error of 0.1 mm. Regarding the present results; another source of error may have decreased our procedure accuracy. As pointed out by several authors [5,26], the relationship between the manipulator end-effector coordinate system and the attached segment coordinate system (humerus coordinate system in our case) may be subject to errors. The rigid transformation between these two coordinate systems has been estimated in the literature by the use of custom fixtures [26] or by an identification procedure using an optical tracking system [5]. In this study, a custom 3D-printed cylinder was rigidly secured on the transected humerus and mounted *via* a custom fixture to the manipulator end-effector. The motions observed on the cylinder were expressed in the end-effector coordinate system under the assumption of fully known rigid transformations (based on the geometry of the different parts) and flush mount joints. While they were not assessed in this study, some errors may have been introduced on these assumptions and should thus be estimated in the future.

Except in several studies investigating foot/ankle dynamics [8,9], most of the previously published joint cadaveric simulators based on a robotic manipulator focused on a single diarthrodial joint. By

proposing an intra-corporal condition procedure, our study made the full kinematic chain of the shoulder girdle available for analysis. As proposed by Oki et al. [1] such a condition opens new opportunities, e.g. by allowing the individual contribution of acromioclavicular and coracoclavicular ligaments to the shoulder kinematics under various humerus motions (i.e. a closer to physiological condition than mobilizing the clavicle while keeping fixed the scapula). This was made possible as robotic manipulators, instead of UTM, are open chain mechanisms that do not limit the explored kinematic chain length. Still, the manipulator has a limited workspace that restrains the potential positions of the exploring bones and joints in the manipulator coordinate system. In robotics, it may be more common to adapt the position of the robot (e.g. mobile manipulator, humanoid robot) than to move the targeted object [27]. In the present study, this issue was managed by optimizing the spatial organization of the specimen with respect to the manipulator to allow requested motions. This procedure, repeated for each shoulder, allowed for the personalization of specimen position and orientation depending on humerus length and humerus range of motion.

Another feature of this study was that our procedure allowed reproducing specimen-specific humerus motions induced by an operator. This procedure simulates intra-operative shoulder passive mobilization performed by the surgeon to assess joint reconstruction or joint arthroplasty efficiency [16]. As observed by Goldsmith et al. [17] using a similar procedure to explore the hip joint, the use of a robotic manipulator allows for reliability in induced motions. However, while these authors used predefined rotation axes to approximately replicate manually-induced motions, our procedure directly uses the recorded manually-induced motions (i.e. the intra-operative shoulder passive mobilization performed by the surgeon) for the robotic motion planning. To the best of our knowledge, this is the first time that specimen-specific motions, recorded during manual passive mobilization, are used for robotic motion planning. Instead, several studies used various motions obtained from open-source datasets compiling records made on healthy participants [5,15,28-31]. The use of specimen-specific motions better allows to respect related joint kinematic constraints (e.g. bony or soft tissue

constraints that may limit further joint motion) and thus to better respect physiologic boundaries. Still, the application of specimen-specific motions recorded during the native condition of a joint may not be applicable in injured or repaired joint conditions, where related joint kinematic constraints may have been modified [17]. Thus, the replication of native humerus motions may not be applied under injured or repaired joint conditions without the monitoring of the resulting passive moment 17 to avoid tissue degradation or joint dislocation. The replication of native humerus motions, though, allows assessing whether the injured or repaired joint still permits the requested motion.

This study remains subject to some limitations. First, all specimens used were over 60 years old. While the shoulders were inspected prior to inclusion in terms of degenerative joint disease or previous ligamentous injury, resulting range of motion may be lower than in younger subjects. Still, the humerus elevation amplitudes reported in this study are similar to the ones reported during *in vivo* studies [32] or cadaveric studies [1]. Second, humerus motions did not include muscle contraction. Consequently, bones kinematics, and in particular scapula kinematics, might not be comparable to the *in vivo* kinematics observed in healthy subjects. However, acromioclavicular joint kinematics observed on cadaveric specimens during passive humerus motions is known to be similar to the joint kinematics measured on healthy participants during active humerus motions [1,33]. Furthermore, the present procedure can be compared to intraoperative joint assessment performed by the surgeon, during full muscle relaxation, as suggested by Goldsmith et al. [17] third, as specimen-specific motions were defined and applied for each shoulder, induced motions may not be perfectly similar between shoulders. Furthermore, without a rigorous humerus mobilization protocol, the resulting motions may not have been perfectly performed around anatomical axes. This issue can be corrected by defining precisely anatomical axes, for example by applying the recommendations of the ISB [4,12]. However, in our case, the goal was more to reproduce intraoperative humerus mobilizations (i.e. not necessarily fully aligned with anatomical axes) than to produce pure rotations around a single axis. Last, the present procedure does not allow for specimen repositioning. The optimized position and orientation applied on the specimen in the manipulator coordinate system remained strictly the same between the manually-induced humerus motions and the following motion replications using the robotic manipulator. Consequently, if the specimen has to be removed and then replaced (e.g. to perform a surgery), the validity of the resulting humerus motion replications cannot be ensured. The literature has already proposed some procedures to cover this issue. However, to the best of our knowledge, they were applied on a unique bony segment, during single diarthrodial joint analysis [26]. Still, these procedures could be applied on the thorax of the specimens to ensure the correct repositioning of the end of the kinematic chain of the shoulder girdle.

Conclusion

To conclude, an advanced joint testing procedure using an industrial redundant robotic manipulator was used to explore the shoulder girdle during specimen-specific humerus motions in native intra-corporal conditions. Using this procedure on 10 shoulders, the manually-induced humerus motions were replicated by the robotic manipulator with high reliability and fidelity. This procedure will be used in the future to explore the native and pathological joint

function as well as to test medical devices, of the shoulder girdle and potentially other joints.

References

1. Oki S, Matsumura N, Iwamoto W, Ikegami H, Kiriya Y, Nakamura T, et al. The function of the acromioclavicular and coracoclavicular ligaments in shoulder motion: A whole-cadaver study. *Am J Sports Med.* 2012;40(11):2617-26.
2. Friis EA, Tsao AK, Topoleski T LD, Jones LC. Introduction to mechanical testing of orthopedic implants. Elizabeth Friis Edi. 2017;3-15.
3. Topoleski T LD, Tsao AK, Friis EA, Jones LC. Introduction to mechanical testing of orthopedic implants. Elizabeth Friis Edi. 2017;33-47.
4. El Daou H, Geoffrey Ng KC, Van Arkel R, Jeffers J RT, Y Baena FR. Robotic hip joint testing: Development and experimental protocols. *Med Eng Phys.* 2019;63:57-62.
5. Aliaj K, Feeney GM, Sundaralingam B, Hermans T, Bo Foreman K, N Bachus K, et al. Replicating dynamic humerus motion using an industrial robot. *PLoS One.* 2020;15(11):e0242005.
6. Lee J, El-Daou H, Alkoheji M, Carlos A, Di Mascio L, Andrew A, et al. Ligamentous and capsular restraints to anterior-posterior and superior-inferior laxity of the acromioclavicular joint: A biomechanical study. *J Shoulder Elbow Surg.* 2021;30(6):1251-6.
7. Smith T, Banker A, Kramer M, Hurschler C, Kaufmann M, Pastor MF, et al. Biomechanical evaluation of inferior scapula notching of reverse shoulder arthroplasty depending on implant configuration and scapula neck anatomy. *Int J Shoulder Surg.* 2015;9(4):103-9.
8. Noble Jr LD, Colbrunn RW, Lee DG, van den Bogert AJ, Davis BL. Design and validation of a general purpose robotic testing system for musculoskeletal applications. *J Biomech Eng.* 2010;132(2):025001.
9. Spivey W, O'Cain C, Gepner B, Spratley E, Kerrigan J. 15th Annual Injury Biomechanics Symposium. 2019.
10. Duprey S, Naaim A, Moissenet F, Begon M, Cheze L. Kinematic models of the upper limb joints for multibody kinematics optimisation: An overview. *J Biomech.* 2017;62:87-94.
11. Pastor MF, Kraemer M, Wellmann M, Hurschler C, Smith T. Anterior stability of the reverse shoulder arthroplasty depending on implant configuration and rotator cuff condition. *Arch Orthop Trauma Surg.* 2016;136(11):1513-9.
12. Wu G, van der Helm FCT, DirkJan Veeger HE, Makhosous M, Van Roy P, Anglin C, et al. ISB recommendation on definitions of joint coordinate systems of various joints for the reporting of human joint motion -- Part II: shoulder, elbow, wrist and hand. *J Biomech.* 2005;38(5):981-92.
13. van Arkel RJ, Jeffers J RT. *In vitro* hip testing in the international society of biomechanics coordinate system. *J Biomech.* 2016;49(16):4154-8.
14. Leardini A, Chiari L, Croce UD, Cappozzo A. Human movement analysis using stereophotogrammetry: Part 3. Soft tissue artifact assessment and compensation. *Gait Posture.* 2005;21(2):212-25.
15. Bates NA, Nesbitt RJ, Shearn JT, Myer GD, Hewett TE. A novel methodology for the simulation of athletic tasks on cadaveric knee joints with respect to *in vivo* kinematics. *Ann Biomed Eng.* 2015;43(10):2456-66.
16. Verstraete MA, Conditt MA, Parsons IM, Greene AT, Roche CP, Decerze J, et al. Assessment of intraoperative joint loads and mobility in reverse total shoulder arthroplasty through a humeral trial sensor. *Semin Arthroplasty.* 2020;30(1):2-12.
17. Goldsmith MT, Rasmussen MT, Turnbull TL, Trindade C AC, LaPrade RF, Philippon MJ, et al. Validation of a six degree-of-freedom robotic system for hip *in vitro* biomechanical testing. *J Biomech.* 2015;48(15):4093-100.
18. KUKA. 2017.

19. Dumas R, Wojtusik J. Estimation of the body segment inertial parameters for the rigid body biomechanical models used in motion analysis. *Handbook of Human Motion*. 2017. pp:1-31.
20. Serge Van Sint Jan. *Color atlas of skeletal landmark definitions*. Churchill Livingstone/Elsevier. 2007.
21. Quigley M, Conley K, Gerkey B, Faust J, Foote T, Leibs J, et al. ROS: an open-source robot operating system. In *ICRA workshop on open source software*. 2009;3(5).
22. Hennemersperger C, Fuerst B, Virga S, Zettinig O, Frisch B, Thomas N, et al. Towards MRI-based autonomous robotic US acquisitions: A first feasibility study. *IEEE Trans Med Imag*. 2017;36(2):538-48.
23. Sakoe H, Chiba S. Dynamic programming algorithm optimization for spoken word recognition. *IEEE Transactions on Acoustics, Speech, and Signal Processing*. 1978;26(1):43-9.
24. Smith MV, Costic RS, Allaire R, Schilling PL, Sekiya JK. A biomechanical analysis of the soft tissue and osseous constraints of the hip joint. *Knee Surg Sports Traumatol Arthrosc*. 2014;22(4):946-52.
25. Darcy SP, Gil JE, Woo SL, Debski RE. The importance of position and path repeatability on force at the knee during six-DOF joint motion. *Med Eng Phys*. 2009;31(5):553-7.
26. El Daou H, Lord B, Amis A, y Baena FR. Assessment of pose repeatability and specimen repositioning of a robotic joint testing platform. *Med Eng Phys*. 2017;47:210-13.
27. Zacharias F, Borst C, Hirzinger G. *IEEE/RSJ International Conference on Intelligent Robots and Systems*. 2007;3229-36.
28. Baxter JR, Sturnick DR, Demetracopoulos CA, Ellis SJ, Deland JT. Cadaveric gait simulation reproduces foot and ankle kinematics from population-specific inputs. *J Orthop Res*. 2016;34(9):1663-8.
29. Herfat ST, Boguszewski DV, Shearn JT. Applying simulated *in vivo* motions to measure human knee and ACL kinetics. *Ann Biomed Eng*. 2012;40(7):1545-53.
30. Sharkey NA, Hamel AJ. A dynamic cadaver model of the stance phase of gait: Performance characteristics and kinetic validation. *Clin Biomech*. 1998;13(6):420-33.
31. Richter H, Simon D, Smith WA, Samorezov S. Dynamic modeling, parameter estimation and control of a leg prosthesis test robot. 2015;39(2):559-73.
32. Ludewig PM, Behrens SA, Meyer SM, Spoden SM, Wilson LA. Three-dimensional clavicular motion during arm elevation: Reliability and descriptive data. *J Orthop Sports Phys Ther*. 2004;34(3):140-9.
33. Teece RM, Lunden JB, Lloyd AS, Kaiser AP, Cieminski CJ, Ludewig PM, et al. Three-dimensional acromioclavicular joint motions during elevation of the arm. *J Orthop Sports Phys Ther*. 2008;38(4):181-90.